

See discussions, stats, and author profiles for this publication at: <https://www.researchgate.net/publication/263942832>

# Nucleation and Crystallization Kinetics of a Multicomponent Lithium Disilicate Glass by in Situ and Real-Time Synchrotron X-ray Diffraction

ARTICLE in CRYSTAL GROWTH & DESIGN · AUGUST 2013

Impact Factor: 4.89 · DOI: 10.1021/cg400835n

---

CITATIONS

9

READS

31

## 5 AUTHORS, INCLUDING:



Saifang Huang

University of Auckland

31 PUBLICATIONS 153 CITATIONS

[SEE PROFILE](#)



Peng Cao

University of Auckland

102 PUBLICATIONS 629 CITATIONS

[SEE PROFILE](#)



Wei Gao

University of Auckland

421 PUBLICATIONS 3,917 CITATIONS

[SEE PROFILE](#)

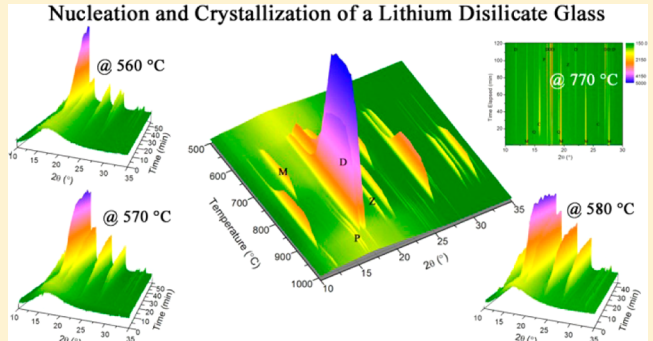
# Nucleation and Crystallization Kinetics of a Multicomponent Lithium Disilicate Glass by in Situ and Real-Time Synchrotron X-ray Diffraction

Saifang Huang,<sup>†,‡</sup> Peng Cao,<sup>\*,†</sup> Ying Li,<sup>†</sup> Zhaohui Huang,<sup>‡</sup> and Wei Gao<sup>†</sup>

<sup>†</sup>Department of Chemical and Materials Engineering, The University of Auckland, PB 92019, Auckland 1142, New Zealand

<sup>‡</sup>School of Materials Science and Technology, China University of Geosciences (Beijing), Beijing 100083, China

**ABSTRACT:** In this study, the high-temperature phase transformation of a multicomponent lithium disilicate glass was investigated by in situ and real-time synchrotron X-ray diffraction in the  $\text{SiO}_2\text{--Li}_2\text{O}\text{--P}_2\text{O}_5\text{--Al}_2\text{O}_3\text{--ZrO}_2$  glass system. Quantitative phase analysis via the Rietveld method was performed on the high-resolution data aiming to reveal the crystallization sequence, crystallization kinetics, and the role of  $\text{P}_2\text{O}_5$  on nucleation. It is found that the nucleation of lithium metasilicate (LS) and lithium disilicate ( $\text{LS}_2$ ) in this complex glass is triggered by the steep compositional gradients associated with the disordered lithium phosphate (LP) precursors in the glass matrix. The  $\text{LS}_2$  crystals grow at the expense of the LS, cristobalite, and quartz phases in the glass during the isothermal crystallization process at 770 °C. The nucleation kinetics is temperature dependent, and the induction period of nucleation is longer at a lower temperature.



## 1. INTRODUCTION

Glass-ceramics with desired properties can be produced by designing a glass recipe and controlling crystallization of the parent glasses.<sup>1</sup> There have been extensive fundamental studies on the mechanisms, kinetics, and thermodynamics of nucleation and crystallization of base glasses.<sup>2–10</sup> The  $\text{Li}_2\text{O}\text{--SiO}_2$  glass systems are one of the most extensively investigated glasses since its discovery in the 1950s.<sup>11,12</sup> In the regime of  $\text{Li}_2\text{O}\text{--SiO}_2$  systems, stoichiometric binary  $\text{Li}_2\text{O}\text{--2SiO}_2$  glass serves as an ideal model material for studying nucleation mechanism and primary phase formation,<sup>2,5,13,14</sup> while multicomponent glasses have been developed for various engineering applications.<sup>9,15</sup> The addition of some indispensable, either minor or major, constituents significantly alters the nucleation and crystallization kinetics and/or phase formation scenarios, which in most cases are more complex than those in the binary  $\text{Li}_2\text{O}\text{--SiO}_2$  systems.

$\text{P}_2\text{O}_5$  is one of the most widely used nucleating agents for glass. McMillan and Partridge<sup>16,17</sup> first discovered the nucleating potency of  $\text{P}_2\text{O}_5$  in a number of ternary glass compositions, such as  $\text{Li}_2\text{O}\text{--Al}_2\text{O}_3\text{--SiO}_2$ ,  $\text{Li}_2\text{O}\text{--MgO}\text{--SiO}_2$ , and  $\text{MgO}\text{--Al}_2\text{O}_3\text{--SiO}_2$ . Due to a charge difference between the two network-forming ions,  $\text{P}^{5+}$  and  $\text{Si}^{4+}$ , one phosphorus–oxygen bond per  $[\text{PO}_4]$  tetrahedron must be a double bond. The presence of this double-bonded oxygen ions leads to a favorable phase separation of phosphate grouping from the silicate network. Follow-up work on adding  $\text{Li}_3\text{PO}_4$  to binary  $\text{Li}_2\text{O}\text{--SiO}_2$  revealed that substitution of 1 mol %  $\text{P}_2\text{O}_5$  for the equivalent amount of  $\text{SiO}_2$  results in significant phase

separation.<sup>18</sup> McMillan et al. also observed that the addition of 1 mol %  $\text{P}_2\text{O}_5$  resulted in a much finer grained microstructure.<sup>19,20</sup>

The works prior to the late 1980s have been summarized in the literature.<sup>11,21</sup> Significant efforts have been devoted to understanding the mechanisms by which  $\text{P}_2\text{O}_5$  addition controls crystallization in glass. One plausible model is epitaxial growth of the crystallizing phase on the nucleating agent or on a phase that incorporates it. Conceptually this model is supported by the close lattice match (i.e., small lattice disregistry) between  $\text{Li}_3\text{PO}_4$  and  $\text{Li}_2\text{Si}_2\text{O}_5$  crystals. The first piece of experimental evidence in favor of this model was given by Headley and Loehmann in 1984.<sup>22</sup> They observed epitaxial growth of cristobalite ( $\text{SiO}_2\text{:CR}$ ), lithium metasilicate ( $\text{Li}_2\text{SiO}_3\text{:LS}$ ), and lithium disilicate ( $\text{Li}_2\text{Si}_2\text{O}_5\text{:LS}_2$ ) on the lithium phosphate ( $\text{Li}_3\text{PO}_4\text{:LP}$ ) crystals. In their work,<sup>22</sup> well-crystallized LP precipitation had been obtained by an initial high temperature treatment at 1000 °C for 20 min, prior to their crystallization study. It is therefore questionable whether LP actually nucleates the silicate phases. Using X-ray diffraction (XRD), Iqbal et al. detected crystallization of  $\text{Li}_3\text{PO}_4$  phase in a  $\text{Li}_2\text{O}\text{--SiO}_2$  system containing 5 mol %  $\text{P}_2\text{O}_5$  when the glass was heated at 476 °C.<sup>23</sup> However, their transmission electron microscopy (TEM) work did not provide direct evidence of the presence of LP. Furthermore, they found that in a glass system

Received: May 29, 2013

Revised: July 5, 2013

Published: July 31, 2013

containing less than 3 mol %  $P_2O_5$ , such LP crystals could not be detected by XRD and TEM if the glass is nucleated in an optimal temperature range (450–550 °C).<sup>23</sup> Due to the technical difficulties of laboratory XRD and microscopy in detecting crystalline phases as they are either in small quantity or small size, the fundamental understanding of the crystallization process is incomplete, and the real role of  $Li_3PO_4$  as a nucleating agent is still unclear.

In addition to the conventional laboratory XRD, microscopy, differential thermal analysis (DTA), and physical property measurements, nuclear magnetic resonance (NMR) has been performed to give a quantitative description of silicate framework species, its interaction with Li ions, and the structural changes of the minor constituents such as P and Si.<sup>23–27</sup> Most recently, Bischoff et al.<sup>28</sup> revisited the crystallization process in a lithium disilicate glass using Si single and double resonance solid state NMR spectroscopy. Their NMR results negate the epitaxial growth model previously proposed by Headley and Loehmann<sup>22</sup> and instead suggest that the nucleation of LS and  $LS_2$  both initiate at the phase boundary between the disordered LP and glass matrix. However, both Headley et al.<sup>22</sup> and Bischoff et al.<sup>28</sup> were unable to reveal what relationship exists between LS and  $LS_2$  during nucleation and crystal growth.

In the past decades, thermodynamic and kinetic aspects of nucleation and crystal growth have been extensively investigated, particularly in simple glass systems.<sup>8</sup> In most cases, the crystallization kinetics follows the well-known Avrami equation, or more accurately KM–JMA equation,<sup>29–31</sup> named after Russian mathematician Kolmogorov and metallurgist Mirkin and American metallurgists Johnson, Mehl, and Avrami. Due to the experimental difficulties in obtaining high-quality nucleation data by the conventional methods such as DTA or laboratory XRD,<sup>7</sup> the understanding of the crystallization kinetics in complex lithium disilicate glasses is still limited.

In this work, we employed X-ray powder diffraction in using synchrotron radiation to reveal the structural changes of the parent glasses *in situ* and in real-time by monitoring spontaneous change in the XRD spectra during glass crystallization. With the high-resolution XRD data, we revisited the nucleation and crystallization processes by quantitatively analyzing the changes of fraction and crystallite size of each phase during both nonisothermal and isothermal crystallization processes, from the very beginning of nucleation to the completion of crystallization. Specifically, the nucleation and crystallization kinetics are investigated in this study.

## 2. EXPERIMENTAL PROCEDURE

In this study, a multicomponent lithium disilicate glass containing both  $P_2O_5$  and  $ZrO_2$  was employed, which has already been documented in the literature.<sup>15,32,33</sup> The nominal composition of this glass were 68.9  $SiO_2$ , 27.5  $Li_2O$ , 1.4  $Al_2O_3$ , 1.9  $P_2O_5$ , and 0.3  $ZrO_2$  (in mol %). The glass was melted in a Pt crucible at 1500 °C for 3 h. Some minor additives such as flux agents ( $K_2O$ ) and colorants were added in the melt. The melt was then shaped into glass rods 10 mm in diameter and 300–400 mm long. Rectangular disc samples (dimensions: 5 × 5 × 0.4) for synchrotron XRD analysis were sliced from the glass rods.

*In situ* high-temperature X-ray diffraction (HT-XRD) was performed on the powder diffraction (PD) beamline at the Australian Synchrotron Centre. An Anton Paar HTK-2000 strip furnace and a Mythen II microstrip detector were attached to

the state-of-the-art synchrotron beamline. The high-resolution data collection was on the Bragg–Brentano diffraction configuration, using X-ray beam energy of 11 keV with a corresponding wavelength of 0.11270 nm. To ensure complete detector coverage, pairs of data sets (p1 and p2) were collected at two detector settings, 0.5° apart. In our case, p1 covered a  $2\theta$  angle from 6.18° to 86° while p2 covered 6.68° to 86.5°, respectively. After data collection, the pairs of data sets merged to remove the gaps that resulted from the spacing between detector modules. Three series of experiments were conducted to study the nucleation and crystallization kinetics of the lithium disilicate glass (Figure 1).

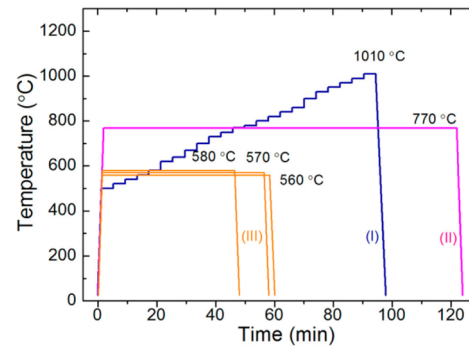


**Figure 1.** The temperature profiles of three series of synchrotron XRD experiments. Series I: continuous heating from 500 to 1010 °C. Series II: isothermal annealing at 770 °C for 120 min, to study crystallization kinetics. Series III: isothermal annealing at 560 °C, 570 °C, and 580 °C, respectively, to study its nucleation kinetics.

**2.1. Nonisothermal Crystallization by Continuously Heating to 1010 °C.** A glass sample was quickly heated from room temperature (~25 °C) to 500 °C in 1 min and then continuously heated to 1010 °C with a ramp rate of 400 K/min in a stepwise manner. The fast ramp rate was employed to minimize the additional nucleation or crystal growth during the heating process. The XRD patterns were continuously recorded from 500 to 1010 °C at an interval from 10 to 30 °C. At each temperature, the sample was held for 4 min for XRD recording.

**2.2. Isothermal Crystallization at 770 °C.** To study the crystallization kinetics, the lithium disilicate glass was heated to a crystallization temperature of 770 °C with a ramp rate of 400 K/min and then held at this temperature for up to 120 min. A total of 200 patterns were recorded during the 120 min holding period.

**2.3. Isothermal Nucleation Kinetics Study at 560–580 °C.** The glass samples were heated from room temperature to a temperature of 560–580 °C. When the temperature reached the prescribed setting, the XRD data were collected. All data were automatically recorded for a fixed collecting time of 30 s (at 560 and 570 °C) or 45 s (at 580 °C) per data set. This ensures achieving high quality spectra and real-time measurements.

A software MAUD, written by Lutterotti on the basis of the full-pattern analysis using the Rietveld method<sup>34</sup> was employed for quantitative phase analysis. For such refinements, a Delf line broadening model was used, adopting an iterative least-squares procedure by minimizing the residual parameters,  $R_{wp}$ ,  $R_B$ , and  $R_{exp}$ . The crystallite size and the microstrain (root-mean-square, r.m.s. strain,  $\langle \epsilon^2 \rangle^{1/2}$ ) were evaluated using an isotropic size-strain model.

The entire suite of data sets was refined sequentially, and crystallinity, volume fraction, and crystallite size of each phase were obtained as a function of temperature and holding time. The information retrieved was then used to investigate the phase formation, nucleation, and crystallization kinetics.

### 3. RESULTS

#### 3.1. Series I: In situ Nonisothermal Crystallization.

Figure 2 shows the synchrotron HT-XRD data of the lithium

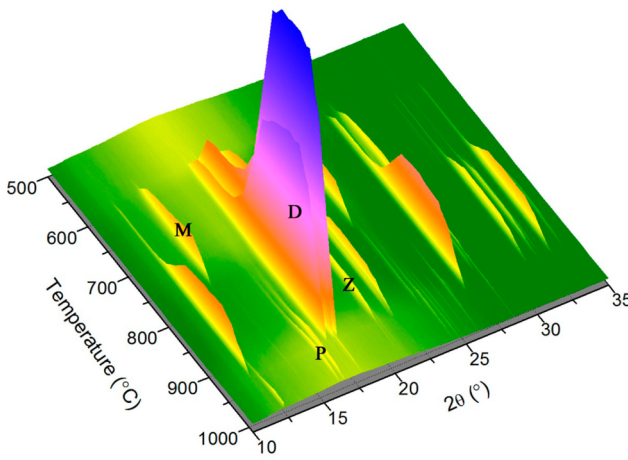


**Figure 2.** Synchrotron HT-XRD of the lithium disilicate glass when continuously heated from 500 to 1010 °C. D:  $\text{Li}_2\text{Si}_2\text{O}_5$  ( $\text{LS}_2$ ); M:  $\text{Li}_2\text{SiO}_3$  (LS); P:  $\text{Li}_3\text{PO}_4$  (LP); Z:  $\text{ZrO}_2$ .

disilicate glass recorded from 500 to 1010 °C (series I). The intensity change of each phase with temperature and/or holding time qualitatively reflects the trend of its volume fraction in the glass samples. In this regard, the strongest peak intensity of each phase (i.e., (111) for  $\text{LS}_2$ , LS, ZrO<sub>2</sub> and (120) for LP) is shown in Figure 3 as a function of temperature.

As presented in Figures 2 and 3, the intensity of the LS phase increases sharply from 580 to 640 °C and then gradually to 750 °C, after which the intensity decreases quickly and vanishes at 780 °C. In contrast, the  $\text{LS}_2$  intensity drastically increases at 730–780 °C and then levels off until 850 °C, followed by a quick decrease and complete vanishing at 950 °C. The ZrO<sub>2</sub> intensity demonstrates a similar trend to the  $\text{LS}_2$ . It seems that when the LP intensity rapidly increases at 850 °C, the LS intensity starts to drop.

A close-up XRD pattern (Figure 4) reveals that the LS peaks emerged at 560 °C while the  $\text{LS}_2$  peaks emerged at 580 °C, suggesting that LS nucleates slightly prior to  $\text{LS}_2$ . This is a new finding in terms of phase transition sequence as most laboratory XRD investigations are unable to identify this sequence in such a narrow temperature range.

**3.1.1. Volume Fraction vs Annealing Temperature.** The p1 pattern of each XRD data set was used for full pattern analysis by Rietveld refinement. Figure 5 presents the temperature-dependent volume fraction of each phase evolved during the continuous heating process (series I). This agrees with the qualitative analysis results in Figure 3. As shown in Figure 5, in the temperature range of 560 to 750 °C, the volume fraction of the LS phase is greater than that of the  $\text{LS}_2$  phase. At a temperature between 750 and 780 °C, the volume fraction of the LS phase rapidly decreases to 0.6 vol %, whereas the  $\text{LS}_2$  phase increases dramatically from 23.4 vol % to 66.6 vol %.

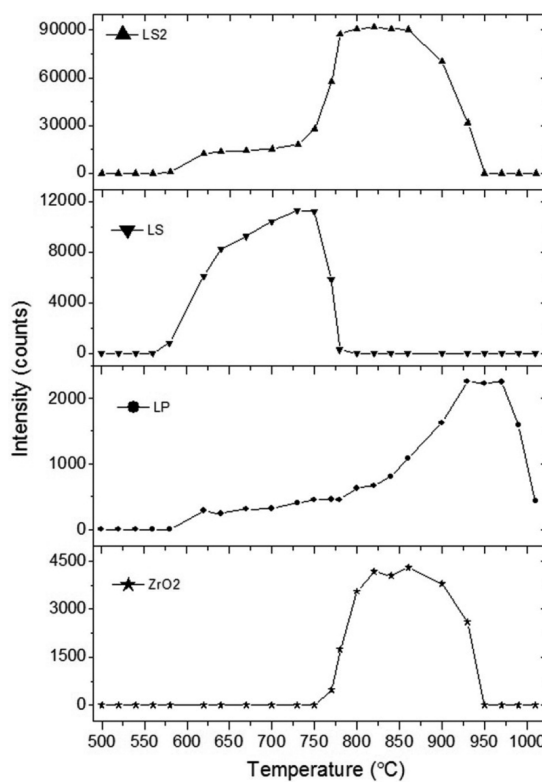


**Figure 3.** Intensities of phases in the series I sample as a function of temperature. The intensity data are taken from the strongest peak of each phase [i.e., (111) plane of  $\text{LS}_2$ , LS, and  $\text{ZrO}_2$  and (120) of LP].

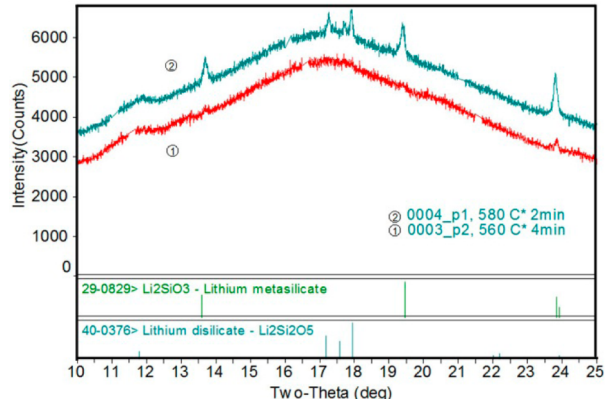


**Figure 4.** The initiation of  $\text{Li}_2\text{SiO}_3$  and  $\text{Li}_2\text{Si}_2\text{O}_5$  phases of series I.

Above 780 °C, the glass-ceramic contains crystalline phases of LS<sub>2</sub>, LP, and ZrO<sub>2</sub>. With increasing temperature, the fraction of the LS<sub>2</sub> phase decreases, whereas that of the LP phase is almost constant before 950 °C. It must be pointed out that the X-ray diffractogram of the LP phase below 780 °C is a broad hump, which can be attributed to the disordered (amorphous) LP species. The formation of such disordered species may be due to the clustering of phosphorus and lithia in the glass matrix. Nevertheless, it is observed that such disordered LP species tends to become ordered when temperature increases and eventually the well-ordered LP crystals form at a temperature of >780 °C.<sup>31</sup> P MAS NMR results by Bischoff et al.<sup>28</sup> present a similar phenomenon. The volume fraction of the ZrO<sub>2</sub> phase is significantly small (refer to the inset in Figure 5). The highest amount of ZrO<sub>2</sub> is 0.73 vol % at 820 °C.

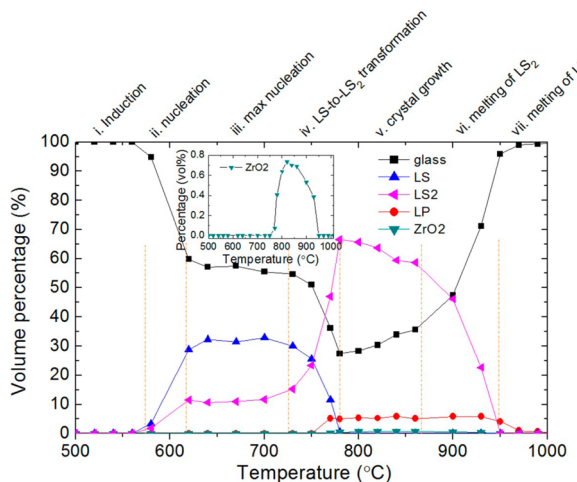


**Figure 5.** Volume fraction of phases as a function of temperature, determined by XRD full pattern quantitative phase analysis.

Nevertheless, it has a similar relationship with temperature as the LS<sub>2</sub> phase does in the range 770–930 °C.

**3.1.2. Crystallite Size vs Annealing Temperature.** Our previous research shows that the well-crystallized LS and LS<sub>2</sub> phases are of the short rod-shape variety in this glass-ceramic.<sup>33</sup> In order to evaluate the crystal growth rate during the crystallization process, the mean crystallite sizes of LS, LS<sub>2</sub>, and LP were determined using an isotropic size-strain model during the Rietveld refinement process, and the results are shown in Figure 6. It is noted that the holding time at each temperature

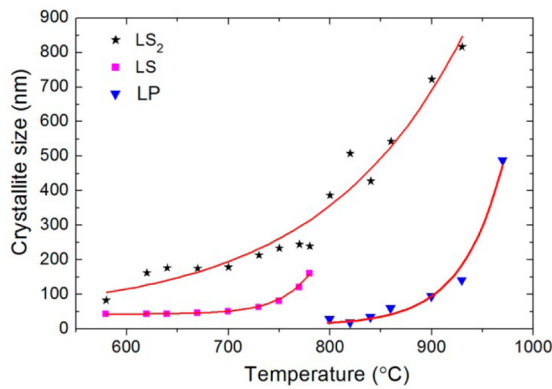


**Figure 6.** Crystallite sizes of LS, LS<sub>2</sub>, and LP phases as a function of temperature.

was 4 min during the XRD data acquisition. It can be seen that the LS<sub>2</sub> crystallite size increases from 83 to 817 nm when the temperature rises from 580 to 930 °C (note that the LS<sub>2</sub> phase disappeared at 950 °C). Concomitantly, the LS crystals grew from 44 to 161 nm as the temperature increased from 580 to 780 °C. In the temperature range of 800 to 950 °C, the LP crystallite size increases from ~25 to ~430 nm. The crystallite sizes of each phase can be fitted to an exponential model as shown in Figure 6.

**3.2. Series II: Real-time isothermal crystallization.** In order to study the crystallization kinetics of this glass, we chose a temperature of 770 °C at which a major LS<sub>2</sub> phase and a certain amount of LS phase exist. Figure 7 displays the synchrotron HT-XRD patterns recorded at this temperature with elapsed time of 120 min. Six phases emerged in the entire

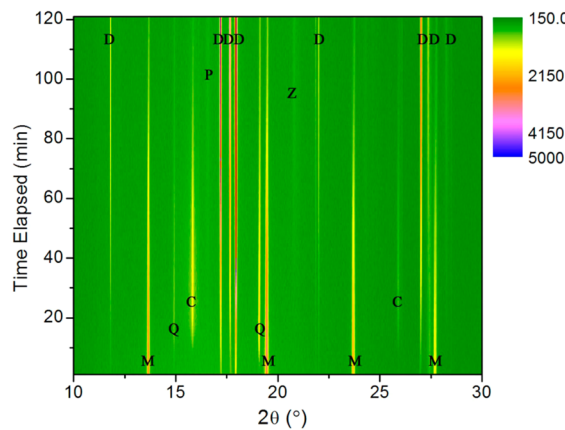


**Figure 7.** Real-time synchrotron HT-XRD of the lithium disilicate glass treated at 770 °C with elapsed time of 120 min, where D: lithium disilicate, Li<sub>2</sub>Si<sub>2</sub>O<sub>5</sub>; P: lithium phosphate, Li<sub>3</sub>PO<sub>4</sub>; M: lithium metasilicate, Li<sub>2</sub>SiO<sub>3</sub>; C: cristobalite; Q: quartz; Z: ZrO<sub>2</sub>. A trace amount of ZrO<sub>2</sub> (<0.15 vol %) precipitated after heating for 24–120 min at this temperature.

process: Li<sub>2</sub>Si<sub>2</sub>O<sub>5</sub> (LS<sub>2</sub>), Li<sub>2</sub>SiO<sub>3</sub> (LS), Li<sub>3</sub>PO<sub>4</sub> (LP), ZrO<sub>2</sub>, cristobalite (CR), and quartz (QZ).

The data shown in Figure 7 were further processed for quantitative phase analysis. The volume fractions of both amorphous and crystalline phases at 770 °C against the time are plotted in Figure 8. Within the first 15 s (when first data set

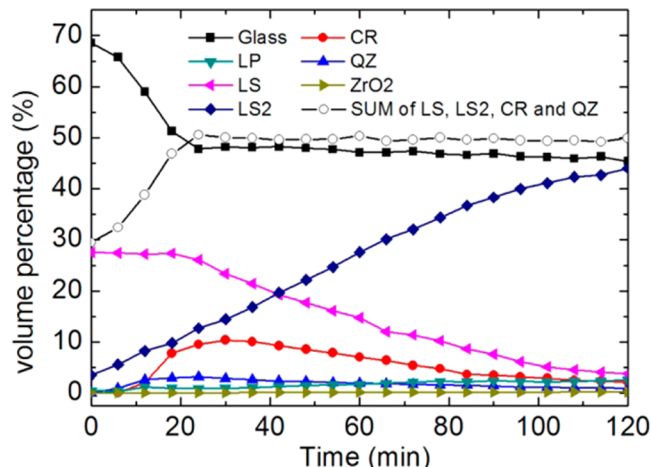


**Figure 8.** Volume fraction of all phases as a function of the elapsed time at 770 °C. The total volume fraction of LS, LS<sub>2</sub>, QZ, and CR against the elapsed time is also plotted.

was recorded), 27.5 vol % LS and 3.5 vol % LS<sub>2</sub> emerged, and the remaining (~70 vol %) was still a glass phase. After the instantaneous advent of LS<sub>2</sub> and LS, the glassy portion decreased quickly from ~70 vol % to less than 50 vol % within the subsequent 24 min. The amount of ~20 vol % glassy phase has been transformed to crystalline LS<sub>2</sub>, cristobalite, and quartz, while the amount of LS phase remains unchanged. After 24 min of holding, the volume fractions of LS, cristobalite, and quartz decreased, while the fraction of LS<sub>2</sub> increased, suggesting that the formation of LS<sub>2</sub> was at the expense of LS, quartz, and cristobalite. This postulation is supported by the fact that the total amount of these four phases did not vary with the holding time (~51 vol % in total).

Apart from the volume fraction change, the crystallite size of the LS and  $LS_2$  phases also changed during the crystallization process. As shown in Figure 9, the  $LS_2$  crystallite size follows a

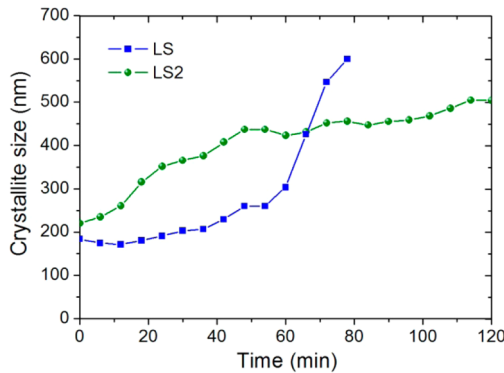


**Figure 9.** Crystal size of the  $LS_2$  and LS phases with the holding time at 770 °C.

power curve, while the LS crystallite size follows an exponential curve. The difference in crystal growth velocity may be ascribed to the different mechanisms of crystal growth for LS and  $LS_2$ .<sup>22</sup> The exponential form of the LS crystallite size curve implies that LS crystal growth proceeds by attaching larger-ordered clusters to the advancing front of LS. These larger-ordered clusters could be formed by phase separation in the glass. On the other hand, the  $LS_2$  growth may be accomplished by single-atom jumping. This different growth mechanisms have been observed in crystallization of Ni–P glass.<sup>35</sup> The crystallite sizes of LS phase after 80 min holding are excluded in Figure 9, due to significant errors in the course of Rietveld refinement.

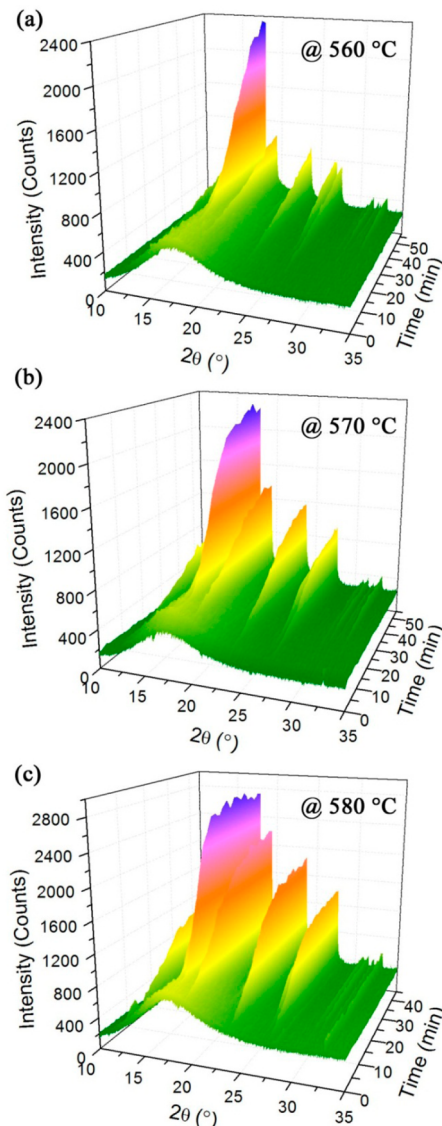
### 3.3. Series III: Real-Time Nucleation Kinetics Study.

Figure 10 shows the real-time synchrotron XRD patterns at 560, 570, and 580 °C. At such a nucleation temperature, only the diffraction peaks of crystalline LS and  $LS_2$  phases were observed. The induction time, within which no nucleation is noticeable, gradually reduces with increasing temperature. For example, at 560 °C noticeable LS peaks emerge after 10 min, while at 580 °C the LS peaks become visible after 3 min.

The volume fraction of the  $LS_2$  and LS phases as a function of nucleation temperature is plotted in Figure 11. At a lower temperature, the induction time of nucleation is longer. All the curves have a typical sigmoidal shape, wherein an initial slow rise is followed by a rapid rise and slows down again toward the completion of crystallization. The LS phase takes a longer time to reach the maximum volume fraction (i.e., saturation state of nuclei) than the  $LS_2$  phase at each nucleation temperature. Besides, the time expected for the saturation of LS nuclei is also much longer at lower temperatures. The kinetics calculation is presented in the subsequent section.

## 4. DISCUSSION

**4.1. Phase Formation Sequence.** **4.1.1. Series I: Non-isothermal Crystallization.** The phase evolution in this glass over temperature can be divided into several stages (Figure 5): (i) induction period, (ii) nucleation of LS and  $LS_2$ , (iii) saturated nucleation stage, (iv) LS-to- $LS_2$  transformation, (v) crystal growth of  $LS_2$  and LP, (vi) melting of  $LS_2$ , and (vii) melting of LP. In this work, we observed the precipitation of  $ZrO_2$  during stages (v) and (vi), even though a trace amount of  $ZrO_2$  (0.73 vol %) was added. LS exists and grows in the



**Figure 10.** Real-time synchrotron HT-XRD patterns of the glass at (a) 560, (b) 570, and (c) 580 °C. The nucleation and crystallization of LS and  $LS_2$  phases are temperature and time dependent.

temperature range from 580 to 930 °C, whereas LS and crystalline LP emerge and grow from 560 to 780 °C and from 780 to 1010 °C, respectively. When the temperature is higher than 1010 °C, the glass is completely melted. The phase formation sequences in the lithium disilicate glass are summarized in Table 1.

On the basis of the observations made in this study and the NMR work of Bischoff et al.<sup>28</sup> whose glass has a similar composition to ours, we propose the following phase formation sequence. At 580–620 °C (stage ii, Figure 5), the crystalline LS is nucleated from  $Q^{(2)}$  (glass) and  $Q^{(3)}$  (glass) via eqs 1 and 2, whereas the formation of  $LS_2$  is probably via eq 3. During 620–730 °C (stage iii), the content and crystallite size of silicate phases have little change.

The observation that LS formed earlier than  $LS_2$  (Figure 4) is in agreement with the nucleation kinetics calculation of LS and  $LS_2$  phases as LS has a lower activation energy.<sup>9</sup> Besides, the evolution of  $LS_2$  in this glass is closely related to LS at 580–780 °C. A more detailed crystallographic study of the glass-ceramic will be reported elsewhere.

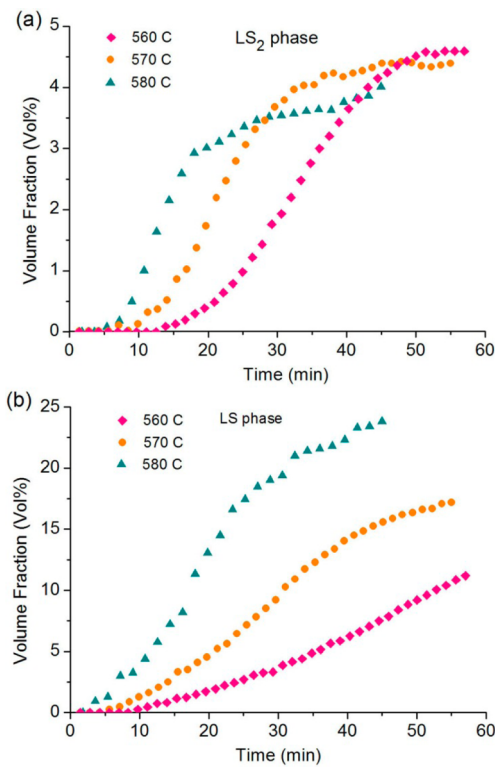


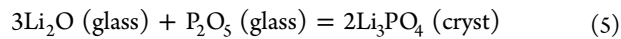
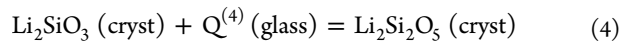
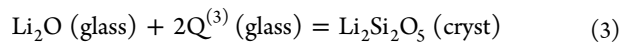
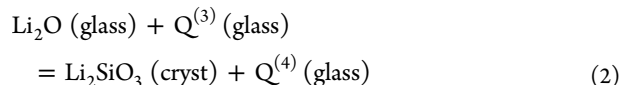
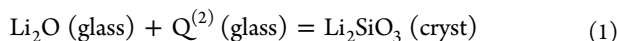
**Figure 11.** Volume fraction of (a) LS<sub>2</sub> and (b) LS phases against the elapsed time at different nucleation temperatures.

**Table 1. Summary of the Phase Formation Sequences in the Lithium Disilicate Glass**

stage	temp range (°C)	reaction sequence
(i)	500–580	induction period of nucleation
(ii)	580–620	nucleation of LS and LS <sub>2</sub>
(iii)	620–730	nuclei of both LS and LS <sub>2</sub> saturated; formation of LP embryos with short-range order (poorly crystallized)
(iv)	740–780	LS-to-LS <sub>2</sub> transformation
(v)	780–860	crystal growth of LS <sub>2</sub> ; formation of LP crystals (well-crystallized); the precipitation of ZrO <sub>2</sub>
(vi)	860–950	melting of LS <sub>2</sub> and ZrO <sub>2</sub>
(vii)	950–1010	melting of LP

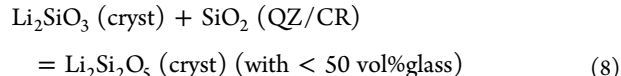
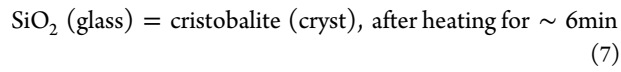
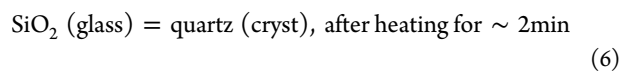
At 740–780 °C (stage iv, Figure 5), the rapid increase of LS<sub>2</sub> and decrease of LS and the glass phase suggest that at this stage, the LS phase likely transforms into the LS<sub>2</sub> phase via eq 4. It is not clear whether or not LP plays a role in promoting the LS-to-LS<sub>2</sub> transition as the well-crystallized LP emerges only at a temperature >800 °C. Subsequently, when the temperature was higher than 800 °C (stages v–vii), the amount of the glass phase starts to increase, while the amounts of LS<sub>2</sub> and ZrO<sub>2</sub> decrease. Also in this temperature range, the LP phase forms via eq 5, and some of the LS<sub>2</sub> and ZrO<sub>2</sub> crystals are melted back to the glass.

LS<sub>2</sub> exists and grows in the range of 580 to 930 °C, whereas LS and crystalline LP emerge and grow from 560 to 780 °C and from 780 to 1010 °C, respectively. When the temperature is higher than 1010 °C, the glass-ceramic is completely melted.



It is noted that the temperature range for the existence of the LS phase is dependent on the glass compositions. In our glass with a SiO<sub>2</sub>/Li<sub>2</sub>O molar ratio of 2.5, the LS phase exists between 580 and 770 °C and disappears at ~780 °C. In the lithium disilicate glass system with the SiO<sub>2</sub>/Li<sub>2</sub>O molar ratio of ~2.8, as reported by Headley et al.,<sup>22</sup> the LS phase remained with a large amount at a higher temperature of 820 °C. Another glass system we recently investigated (SiO<sub>2</sub>/Li<sub>2</sub>O molar ratio of ~2.4)<sup>36</sup> shows that the formation of LS is very limited or even cannot be detected during the entire phase evolution process. Therefore, it is worth pointing out that the formation of LS in a lithium disilicate glass is largely dependent upon the overall glass composition and cannot be merely judged from the molar ratio of SiO<sub>2</sub>/Li<sub>2</sub>O.

**4.1.2. Series II: Isothermal Crystallization.** The Rietveld refinement results reveal the correlation between volume fraction of each phase and holding time at 770 °C (Figure 8). It is found that when the glass was directly heated to 770 °C devoid of a nucleation stage, two silica phases, cristobalite (CR) and quartz (QZ), formed in the sample within a few minutes. The formation of these phases is proposed to be achieved via the reaction eqs 3, 6, 7, and 8.



It is noted from Figure 8 that almost instantaneously, the fraction of LS, LS<sub>2</sub>, and LP reaches 27.5 vol %, 3.5 vol %, and 0.4 vol %, respectively. Due to the significant change in atomic mobility with structural relaxation at 770 °C, these initial amounts of crystallized phases are determined by the phase equilibrium in this glass system (lever rule). The variation of volume fractions of LS<sub>2</sub> (Figure 8) suggests that the formation of LS<sub>2</sub> is at the expense of LS, CR, and QZ via eq 8. This postulation is supported by the fact that the total amount of these four phases does not vary with the holding time (amounting to ~51 vol % in total). The gradually reduced growth rate of LS<sub>2</sub> (Figure 9) could be ascribed to the reduced amounts of the reactants LS, CR, and QZ available in the glass. Besides, the changing composition of the glass is also likely to affect both the thermodynamic and kinetic parameters during crystallization.<sup>10</sup>

It is also noted that the types of silica phase precipitates in this glass depends on the heat treatment procedures. For example, with the isothermal profile of series II, two types of silica phases (QZ and CR) formed. In the same glass, however, only cristobalite precipitated in a conventional annealing process (i.e., separate nucleation and crystallization), as

reported in our previous study,<sup>33</sup> no silica phase formed during the 23-step nonisothermal process of series I. This strongly suggests that the silica phases (quartz and cristobalite) preferably crystallize when a relatively large amount of glassy phase is left in the lithium disilicate glass-ceramics at high temperatures. It is based on the fact that there are sufficient ingredients in the base glass for the formation of various phases in Series II.

In comparison, however, for a nonisothermal annealing process, the formation of silica phases is limited. This is probably because a considerable amount of  $\text{SiO}_2 + \text{Li}_2\text{O}$  ingredients are consumed during the nucleation and crystallization of silicate phases ( $\text{LS}$  and  $\text{LS}_2$ ) at the initial stages. The results also indicate that the properties of glass-ceramics can be tailored via a finely controlled phase transformation process.

**4.2. Role of  $\text{P}_2\text{O}_5$ .** The broad humplike diffraction peak of the LP phase, located at  $2\theta$  angle of  $16^\circ$ – $17^\circ$ , was observed in the high-resolution real-time synchrotron XRD patterns. It is suggested that the  $\text{P}_2\text{O}_5$  species is being transformed to short-range order LP embryos (8–20 nm). LP embryos are poorly crystallized with a disordered structure at 580–770 °C. This is consistent with the NMR findings of Bischoff et al. who suggested that phosphate acts as a lithium ion scavenger via formation of orthophosphate ( $\text{P}^{(0)}$ ) and/or pyrophosphate ( $\text{P}^{(1)}$ ) species.<sup>28</sup> It is probably more accurate to state that the LP phase is amorphous or disordered glassy phase at the nucleation period via eq 5.

The volume fraction of glass phases is drawn in Figure 5. It has two downward trends in the ranges of 560–620 °C and 750–780 °C due to the nucleation and rapid  $\text{LS}$ -to- $\text{LS}_2$  transformation (via eq 4), respectively. Below 780 °C, the disordered structure of the LP glassy phase gradually shifted toward the ordered structure of the crystalline LP phase (~5.5 vol %) and contributed to the phase separation of the silica-rich droplet and lithia-rich matrix phases from the base glass.<sup>37</sup> The boundaries of amorphous LP species were therefore regarded as the nucleation sites for lithium silicate phases. The formation of crystalline LP may contribute to the rapid transformation of  $\text{LS}_2$  from  $\text{LS}$  via eq 4.

From the evolution of the phosphorus species as discussed above, it is suggested that the addition of  $\text{P}_2\text{O}_5$  in the glass results in microstructural heterogeneities and steep compositional gradients in the glass at the early stage of nucleation. These results support the speculation of Höland et al.<sup>1</sup> on the nucleation mechanism and in good agreement with the suggestion of Bischoff et al.<sup>28</sup> It is believed that the nucleation of  $\text{LS}$  and  $\text{LS}_2$  phases in a conventional annealing process, in which no LP crystals are preseeded, is initiated by the disordered phosphorus species.

The cubic zirconia phase crystallized in the glass has little positive contribution to the crystallization of  $\text{Li}_2\text{Si}_2\text{O}_5$  but will hamper the crystal growth, as suggested in the literature.<sup>15,38</sup> This type of zirconia also has no obvious contribution to the mechanical properties of lithium disilicate glass-ceramics.<sup>33</sup>

**4.3. Isothermal Kinetics Investigation.** A simplified expression for the KM-JMA is given by eq 9

$$x(t) = 1 - \exp(-Kt^n) \quad (9)$$

where  $x(t)$  is the volume fraction of a crystalline phase transformed and  $k$  is a rate constant which incorporates the nucleation rate and the rate of radial growth of the newly nucleated nuclei. The value of the Avrami exponent  $n$ , which

varies between 0.5 and 4, provides information on the crystallization mechanism.<sup>39</sup>

In many cases, the sigmoidal shape curves involve an induction period ( $t_0$ ) beyond which nucleation is negligible. As such, a modified formula is usually used and given by eq 10:

$$x(t) = 1 - \exp[-k(t - t_0)^n] \quad (10)$$

By fitting experimental data, the Avrami exponent,  $n$ , and rate constant,  $k$ , for each crystalline phase were calculated and summarized in Table 2. The value of  $n$  for the  $\text{LS}_2$  phase

**Table 2. The Induction Time ( $t_0$ ) and Fitted Avrami Coefficients ( $n$  and  $k$ ) for the Nucleation of  $\text{LS}_2$  and  $\text{LS}$  phases at 560, 570, and 580 °C**

temp (°C)	$\text{LS}_2$			$\text{LS}$		
	$t_0$ (min)	$n$	$\ln k$	$t_0$ (min)	$n$	$\ln k$
560	12.5	1.82	-9.20	8.3	1.49	-7.07
570	5.6	1.74	-8.70	4.2	1.37	-6.77
580	3.6	1.84	-8.27	1.8	1.24	-6.35

(1.74–1.84) is higher than that for the  $\text{LS}$  phase (1.24–1.49), while the rate constant  $k$  of  $\text{LS}_2$  is smaller than that of the  $\text{LS}$  phase. The rate constant,  $k$ , of both the  $\text{LS}_2$  and the  $\text{LS}$  phases increased with increasing temperature.

These data are used to calculate the activation energy with an Arrhenius assumption. The activation energies  $E_a$  of  $\text{LS}_2$  and  $\text{LS}$  are 275 and 213 kJ/mol, respectively, and are relatively smaller than those reported by Hammetter et al. from DTA investigations (i.e., 360 kJ/mol for nucleation of  $\text{LS}_2$  and 270 kJ/mol for  $\text{LS}$ ).<sup>9</sup>

In a similar way, the crystallization kinetics analysis is carried out. The Avrami exponent  $n$  of  $\text{LS}_2$  crystallization is about 0.85. It may suggest that the  $\text{LS}_2$  crystals grow with finite dimensions in assumption of no effects of the external surface.<sup>39</sup> This suggestion is assisted by the microstructure of this glass-ceramic reported previously<sup>33</sup> (i.e.,  $\text{LS}_2$  clusters crystallized with lengths of 0.5–1  $\mu\text{m}$ ) and also by the refined crystallite size of  $\text{LS}_2$  in Figure 9. The LP phase is continuously precipitating as time elapses at 770 °C. The kinetic study shows that its Avrami exponent  $n$  is 0.79.

It has to be noted that the above kinetics analysis is based on an indirect measurement of volume fractions of crystallites. A direct count of crystal number and measurement of their sizes is necessary if the technique permits.

## 5. CONCLUSIONS

The crystallization kinetics of a multicomponent lithium disilicate glass was investigated by *in situ* and real-time synchrotron high-temperature X-ray diffraction (HT-XRD) in the  $\text{SiO}_2$ – $\text{Li}_2\text{O}$ – $\text{P}_2\text{O}_5$ – $\text{Al}_2\text{O}_3$ – $\text{ZrO}_2$  system. With the high-resolution synchrotron XRD data, the effects of temperature and holding time on the phase transformation, crystallite size, and crystallinity was studied by quantitative phase analysis using the Rietveld full-pattern fitting method.

The *in situ* synchrotron HT-XRD experiments have proved that, without precrystallization of lithium phosphate ( $\text{Li}_3\text{PO}_4$ ), the nucleation mechanism of lithium metasilicate ( $\text{Li}_2\text{SiO}_3$ ) and disilicate ( $\text{Li}_2\text{Si}_2\text{O}_5$ ) in the complex lithium disilicate glass were triggered by the steep compositional gradients arising from the disordered lithium phosphate structural units in the glass matrix. This finding is in good agreement with the solid-state NMR results reported by Bishchoff et al. (2011) and is different

from the epitaxial growth mechanism in the glasses with the aid of well-crystallized  $\text{Li}_3\text{PO}_4$  nucleating agent suggested by Headley et al. (1984).

Moreover,  $\text{Li}_2\text{SiO}_3$  was evidenced to nucleate ahead of  $\text{Li}_2\text{Si}_2\text{O}_5$ , rather than simultaneously, at the very beginning of the nucleation of this glass. But it cannot answer whether the nucleation of  $\text{Li}_2\text{Si}_2\text{O}_5$  relied on the preformation of  $\text{Li}_2\text{SiO}_3$ . The crystallinity of this glass reached  $\sim 72.6$  vol % at  $780\text{ }^\circ\text{C}$ . The crystallite size of each phase increased obviously at the corresponding temperature range of the crystal growth stage.

$\text{Li}_2\text{Si}_2\text{O}_5$  continued to grow at the expense of  $\text{Li}_2\text{SiO}_3$ , cristobalite, and quartz when the glass was quickly heated to  $770\text{ }^\circ\text{C}$  and held for 2 h. The volume fractions of the related crystalline phases were fitted according to the KM-JMA model; crystallization of cubic zirconia was modeled with a linear function, and its growth rate is about 0.19 % per minute at  $770\text{ }^\circ\text{C}$ .

The nucleation of the complex lithium disilicate glass was a heterogeneous nonsteady state, and its kinetics was temperature dependent. At a lower temperature, the induction period of nucleation was longer. The volume fractions at different nucleation temperatures were modeled according to a modified KM-JMA equation  $x(t) = 1 - \exp[-k(t-t_0)^n]$  to incorporate the initial induction period. The Avrami exponent ( $n$ ) of  $\text{LS}_2$  phase (1.74–1.84) was higher than that of the LS phase (1.24–1.49), indicating different nucleation mechanisms. The activation energy  $E_a$  of  $\text{LS}_2$  and LS are calculated to be 275 and 213 kJ/mol, respectively.

## AUTHOR INFORMATION

### Corresponding Author

\*Address: 20 Symonds St., Auckland 1010, New Zealand. E-mail: p.cao@auckland.ac.nz. Tel: +64 9 3737 599, ext 86924.

### Notes

The authors declare no competing financial interest.

## ACKNOWLEDGMENTS

This research was undertaken on the Powder Diffraction Beamline at the Australian Synchrotron, Victoria, Australia (project ID: AS121/PDFI/4411). We acknowledge the Beamline Scientists Dr. Qinfen Gu and Dr. Justin Kimpton for their assistance and thank Dr. Tianping Zhu and Dr. Yuxin Wang for help with the synchrotron data collections. S.F.H. would like to acknowledge the China Scholarship Council (CSC) for providing a doctoral scholarship for his Ph.D. study at The University of Auckland.

## REFERENCES

- (1) Höland, W.; Rheinberger, V.; Schweiger, M. *Philos. Trans. R. Soc., A* **2003**, *361*, 575–589.
- (2) Barker, M. F.; Wang, T.-H.; James, P. F. *Phys. Chem. Glasses* **1988**, *29*, 240–248.
- (3) Holand, W.; Rheinberger, V.; Apel, E. *Glass Technol.* **2004**, *45*, 74–77.
- (4) Zanotto, E. D.; Fokin, V. M. *Philos. Trans. R. Soc., A* **2003**, *361*, 591–613.
- (5) James, P. F. *J. Non-Cryst. Solids* **1985**, *73*, 517–540.
- (6) Müller, R.; Zanotto, E. D.; Fokin, V. M. *J. Non-Cryst. Solids* **2000**, *274*, 208–231.
- (7) Fokin, V. M.; Zanotto, E. D.; Yuritsyn, N. S.; Schmelzer, J. W. P. *J. Non-Cryst. Solids* **2006**, *352*, 2681–2714.
- (8) Fokin, V. M.; Yuritsyn, N. S.; Zanotto, E. D. Nucleation and Crystallization Kinetics in Silicate Glasses: Theory and Experiment. In *Nucleation Theory and Applications*; Schmelzer, J. W. P., Ed.; Wiley-VCH: Hoboken, NJ, 2005; pp 74–125.
- (9) Hammetter, W. F.; Loehman, R. E. *J. Am. Ceram. Soc.* **1987**, *70*, 577–582.
- (10) Kelton, K. F.; Greer, A. L., Crystallization in Glasses. In *Pergamon Materials Series*; Kelton, K. F.; Greer, A. L., Eds. Pergamon: Oxford, U.K., 2010; Vol. 15, pp 279–329.
- (11) McMillan, P. W. *Glass-Ceramics*, 2nd ed.; Academic Press: London, 1979.
- (12) Stookey, S. D. *Ind. Eng. Chem.* **1959**, *51*, 805–808.
- (13) Burgner, L. L.; Weinberg, M. C. *J. Non-Cryst. Solids* **2001**, *279*, 28–43.
- (14) Soares, P. C., Jr; Zanotto, E. D.; Fokin, V. M.; Jain, H. *J. Non-Cryst. Solids* **2003**, *331*, 217–227.
- (15) Apel, E.; van't Hoen, C.; Rheinberger, V.; Höland, W. *J. Eur. Ceram. Soc.* **2007**, *27*, 1571–1577.
- (16) Mcmillan, P. W.; Partridge, G. Improvements in or relating to devitrified glass-ceramics and their production. G.B. Patent 924996, 1963.
- (17) Partridge, G.; McMillan, P. W. *Glass Technol.* **1963**, *4*, 173–182.
- (18) Holland, D.; Iqbal, Y.; James, P.; Lee, B. *J. Non-Cryst. Solids* **1998**, *232*–*234*, 140–146.
- (19) Hing, P.; McMillan, P. W. *J. Mater. Sci.* **1973**, *8*, 340–348.
- (20) Harper, H.; James, P. F.; McMillan, P. W. *Discuss. Faraday Soc.* **1970**, *50*, 206–213.
- (21) Lewis, M. H. *Glasses and Glass-Ceramics*; Chapman & Hall: London, 1989.
- (22) Headley, T. J.; Loehman, R. E. *J. Am. Ceram. Soc.* **1984**, *67*, 620–625.
- (23) Iqbal, Y.; Lee, W. E.; Holland, D.; James, P. F. *J. Mater. Sci.* **1999**, *34*, 4399–4411.
- (24) Dupree, R.; Holland, D.; Mortuza, M. G. *J. Non-Cryst. Solids* **1990**, *116*, 148–160.
- (25) Fernandes, H.; Tulyaganov, D.; Goel, A.; Ferreira, J. *J. Therm. Anal. Calorim.* **2011**, *103*, 827–834.
- (26) Mortuza, M.; Ahsan, M.; Dupree, R.; Holland, D. *J. Mater. Sci.* **2007**, *42*, 7950–7955.
- (27) Sen, S.; Gerardin, C.; Navrotsky, A.; Dickinson, J. E. *J. Non-Cryst. Solids* **1994**, *168*, 64–75.
- (28) Bischoff, C.; Eckert, H.; Apel, E.; Rheinberger, V. M.; Holand, W. *Phys. Chem. Chem. Phys.* **2011**, *13*, 4540–4551.
- (29) Johnson, W. A.; Mehl, R. F. *Trans. AIME* **1939**, *135*, 416–442.
- (30) Hillert, M. *Metall. Mater. Trans. A* **2011**, *42*, 3241–3241.
- (31) Barmak, K. *Metall. Mater. Trans. B* **2010**, *41*, 2711–2775.
- (32) Höland, W.; Apel, E.; van't Hoen, C.; Rheinberger, V. *J. Non-Cryst. Solids* **2006**, *352*, 4041–4050.
- (33) Huang, S.; Zhang, B.; Huang, Z.; Gao, W.; Cao, P. *J. Mater. Sci.* **2013**, *48*, 251–257.
- (34) Lutterotti, L.; Matthies, S.; Wenk, H.-R. *International Union of Crystallography: Commission for Powder Diffraction Newsletter* **1999**, *21*, 14–15.
- (35) Lu, K.; Wang, J. T. *J. Cryst. Growth* **1989**, *94*, 448–454.
- (36) Huang, S.; Cao, P.; Wang, C.; Huang, Z.; Gao, W. *J. Asian Ceram. Soc.* **2013**, *1*, 46–52.
- (37) O'Donnell, M. D.; Hill, R. G.; Karpukhina, N.; Law, R. V. *Dent. Mater.* **2011**, *27*, 990–996.
- (38) Goswami, M.; Kothiyal, G. P.; Montagne, L.; Delevoye, L. *J. Solid State Chem.* **2008**, *181*, 269–275.
- (39) Christian, J. W. *The Theory of Transformation in Metals and Alloys*, 3rd ed.; Pergamon: Oxford, 2002.